Journal of the Australian Ceramic Society (2021) 57:597–604
https://doi.org/10.1007/s41779-021-00566-5

RESEARCH

Synthesis, characterization, and UV light-driven photocatalytic properties of $CeVO_4$ nanoparticles synthesized by sol-gel method

Anukorn Phuruangrat[1] · Somchai Thongtem[2,3] · Titipun Thongtem[3,4]

Received: 5 July 2020 / Revised: 22 November 2020 / Accepted: 14 January 2021 / Published online: 21 January 2021

Abstract

$CeVO_4$ as UV light-driven photocatalyst was synthesized by sol-gel method using tartaric acid as a complexing reagent with subsequent calcination at 450–600 °C for 2 h in ambient air. The as-synthesized products were characterized by thermogravimetric analysis (TGA), X-ray diffraction (XRD), scanning electron microscopy (SEM), transmission electron microscopy (TEM), Fourier transform infrared spectroscopy (FTIR), and Raman spectroscopy. The precursor shows two weight loss steps due to the evaporation and decomposition of absorbed water, tartaric acid, and nitrate constituent until at a temperature above 450 °C. XRD patterns of the samples were indexed to *tetragonal* zircon-type $CeVO_4$ structure. The degree of crystallinity and size of the $CeVO_4$ sample were increased by the high growth rate of $CeVO_4$ nanoparticles at high temperature calcination. Particle sizes of the products were 20–40 nm for $CeVO_4$ with 450 °C calcination and 80–120 nm for $CeVO_4$ with 500 °C calcination. The detection of V–O and Ce–O stretching modes indicates the formation of *tetragonal* zircon-type $CeVO_4$ structure. The photocatalytic activity of the as-synthesized $CeVO_4$ nanoparticles was evaluated via the degradation of methylene blue (MB) under UV light irradiation. In this research, $CeVO_4$ with 450 °C calcination showed the highest photocatalytic activity of 94.58% within 120 min under UV light irradiation because of the highest available surface active sites for photodegradation of MB under UV light irradiation.

Keywords $CeVO_4$ nanoparticles · Sol-gel method · Photocatalysis · Spectroscopy

Introduction

In recent years, nanomaterials are much attractive and are extensively potential application in different fields such as catalysis, magnetic properties, biosensors, information storage, and morphology dependent on chemical and physical properties controlled by their size, shape, morphology, and surface state as compared with bulk counterpart [1–3]. The surface area to volume ratio of nanoparticles is very high. Thus, they exhibit structural stabilities, prominent spatial uniformity, and more reactive sites as compared with larger particles and bulk counterpart [1, 4, 5].

Rare earth metal-based orthovanadate (AVO_4) such as $LaVO_4$, $PrVO_4$ and $NdVO_4$ as the important materials show potential application in different fields such as lithium-ion batteries, humidity sensors, catalysis, solar cells, gas sensors, microwave application, photoluminescence, scintillation materials and optical fibers [1, 6–8]. They have long been viewed as promising system in optoelectronic technology for laser application because of the strong absorption of VO_4^{3-} group and efficient energy transfer [7, 8]. Among them, $CeVO_4$ as a zircon-type tetragonal material is an important member of rare earth metal orthovanadate which has been widely used for catalysis, solar cells, magnetic and optoelectronic nanodevices, and biochemical tags [6, 7, 9]. It shows high catalytic activity for dehydrogenation of propane at low temperature. It also represents a new class of optically inactive material used as counter electrode [2, 6].

✉ Anukorn Phuruangrat
phuruangrat@hotmail.com

✉ Titipun Thongtem
ttpthongtem@yahoo.com

[1] Department of Materials Science and Technology, Faculty of Science, Prince of Songkla University, Hat Yai, Songkhla 90112, Thailand

[2] Department of Physics and Materials Science, Faculty of Science, Chiang Mai University, Chiang Mai 50200, Thailand

[3] Materials Science Research Center, Faculty of Science, Chiang Mai University, Chiang Mai 50200, Thailand

[4] Department of Chemistry, Faculty of Science, Chiang Mai University, Chiang Mai 50200, Thailand

$CeVO_4$ nanostructure has been prepared using different methods such as solid state reaction [10, 11], hydrothermal process [12, 13], precipitation [14, 15], microwave method [16, 17], and sol-gel [18]. Sol-gel method was chosen for the synthesis approach owing to the molecular similarity, possible use of different precursors, ability to dope trace amount of different elements, microstructural property control, high purity crystal under low condition and low cost [18–21].

In this work, $CeVO_4$ samples were synthesized by sol-gel method using tartaric acid as a complexing reagent with the subsequent calcination at 450–600 °C for 2 h in ambient air. Effect of calcination temperature on photocatalytic degradation of methylene blue (MB) under UV light irradiation was investigated. Phase, molecular vibration and morphology of the as-synthesized products were studied by thermogravimetric analysis (TGA), X-ray diffraction (XRD), Raman spectroscopy, Fourier transform infrared (FTIR) spectroscopy, scanning electron microscopy (SEM), and transmission electron microscopy (TEM). They found that $CeVO_4$ with 450 °C calcination shows the highest photocatalytic activity for MB degradation due to its smallest particle and highest surface area. The photocatalytic stability of reused $CeVO_4$ was investigated for five cycles. The role of active species for photodegradation of MB over $CeVO_4$ was intensively studied and discussed.

Experiment

Cerium(III) nitrate hexahydrate ($Ce(NO_3)_3{\cdot}6H_2O$, 99.99% trace metal basis), ammonium metavanadate (NH_4VO_3, ACS reagent, ≥ 99.0%), and tartaric acid ($C_4H_6O_6$, ACS reagent, ≥ 99.5%) purchased from Sigma-Aldrich Corporation, and methylene blue ($C_{16}H_{18}ClN_3S$, 95.0-10TiO1.0%) purchased from LobaChemie Pvt Ltd were used without further purification.

$CeVO_4$ as UV light-driven photocatalyst was synthesized by sol-gel method. 0.005 mol $Ce(NO_3)_3{\cdot}6H_2O$ and 0.005 mol $C_4H_6O_6$ (tartaric acid) were dissolved in 100 ml reverse osmosis (RO) water with being stirred by a magnetic stirrer. Concurrently, 0.05 mol NH_4VO_3 was dissolved in 100 ml RO water under stirring at 80 °C to obtain a clearly yellow solution. The two solutions were mixed and heated at 80 °C under stirring to form homogenous gel. The gel precursor was heated at 120 °C in an electric oven and ground to obtain dried powder. The dried powder was heated at 450–600 °C by a heating rate of 10 °C min^{-1} in ambient air for 2 h to form products for further investigation.

The thermal analysis was characterized by a simultaneous thermal analyzer (STA 8000, PerkinElmer) at T_R–1000 °C with a heating rate of 10 °C min^{-1} in nitrogen atmosphere. X-ray diffraction patterns of samples were obtained from a Rigaku SmartLab X-ray diffractometer using Cu K_α radiation as an X-ray source at a scanning rate of 0.005 °.sec^{-1} within 10 ° – 60 °. Fourier transform infrared spectroscopy (FTIR) was recorded by a Bruker Tensor 27 FTIR at room temperature. The sample was diluted by KBr and recorded over the wavenumber of 400–4000 cm^{-1}. Raman spectrophotometer (Horiba Jobin Yvon T64000) was operated using 30 mW HeNe laser 632.8 nm wavelength. Scanning electron micrographs were taken using a scanning electron microscope (SEM, JEOL JSM 6335F) operating at 20 kV. The samples were dispersed in absolute ethanol by 10-min ultrasonic vibration, dropped on a copper tape attached on aluminum stubs, and dried at room temperature. To prevent charging effect, the samples were gold sputtered by SPI module™ sputter coater before SEM analysis. Transmission electron micrographs were taken using a transmission electron microscope (TEM, JEOL JEM-2100) operating at 200 kV.

Photocatalytic activity was evaluated through the degradation of MB solution. Three 18 W black light lamps were used as a UV source. 0.2 g photocatalyst was added to 200 ml of 1×10^{-5} M MB solution which was homogenized by magnetic stirring. For every 30-min specific time interval, 5 ml solution was withdrawn from the tested solution and centrifuged. The absorbance was measured by a UV-visible spectrophotometer at 664 nm, corresponding to the absorption wavelength of MB. The degradation of MB was calculated using the below equation.

$$Decolorization\ efficiency\ (\%) = \frac{C_o - C_t}{C_o} \times 100 \quad (1)$$

C_o is the initial concentration of MB, and C_t is the concentration of MB after UV light irradiation within the elapsed time (t).

Results and discussion

Thermal analysis of precursor was studied by TGA at T_R–1000 °C with heating rate of 10 °C min^{-1} in nitrogen atmosphere as the results shown in Fig. 1. The TGA curve of precursor shows two weight losses at T_R–210 °C and 210–450 °C. The first weight loss of 12% is associated with the evaporation of absorbed water in the precursor [22–24]. The second weight loss of about 18% is caused by the decomposition of tartaric acid containing in the precursor and nitrate of the starting materials [22–24]. The rate of weight loss was the highest at 200–220 °C. At a temperature higher than 370 °C, TGA curve of precursor shows a slow weight loss and becomes stationary upon reaching the complete formation of final product [22–24]. The thermal analysis of precursor indicates that the suitable calcination temperature should exceed 450 °C. Thus, 450–600 °C range was selected for calcination of the precursor of the present work.

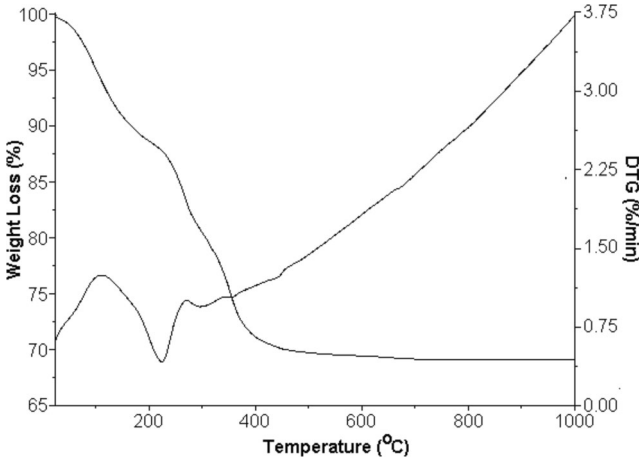

Fig. 1 TGA and DTG curves of precursor at T_R–1000 °C in nitrogen atmosphere

Crystalline structure of the as-synthesized $CeVO_4$ samples with 450–600 °C calcination was analyzed by an X-ray diffractometer at $2\theta = 10^o$–60^o as the results shown in Fig. 2. The XRD patterns exhibit well defined diffraction at $2\theta = 18.18^o$, 24.05^o, 30.33^o, 32.42^o, 34.30^o, 36.84^o, 39.07^o, 43.50^o, 46.40^o, 47.88^o, 49.23^o, 50.41^o, 55.55^o, and 56.64^o which correspond to the (101), (200), (211), (112), (220), (202), (301), (103), (321), (312), (400), (213), (420), and (004) planes of *tetragonal* zircon-type $CeVO_4$ structure of the JCPDS card no. 12-0757 [25], respectively. No impurity peaks were detected in these XRD patterns. They indicate that all samples are good single crystalline phase. Intensity of all diffraction peaks of the samples was increased with increasing in the calcination temperature. The *degree* of

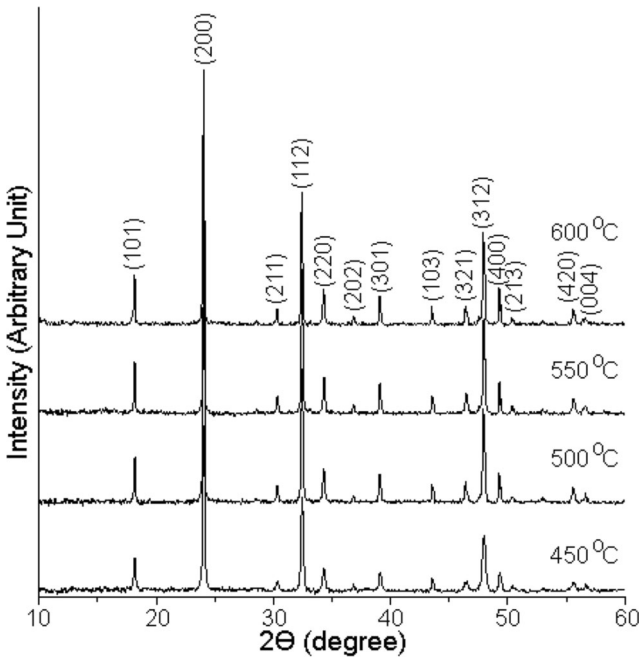

Fig. 2 X-ray diffraction patterns of $CeVO_4$ samples synthesized by sol-gel method and followed by 450–600 °C calcination for 2 h in ambient air

crystallinity and size of the $CeVO_4$ samples are also increased due to the higher growth rate of $CeVO_4$ particles at higher calcination temperature.

Raman spectroscopy was also used to determine crystalline structure of $CeVO_4$ nanoparticles by investigating bonding state of different atoms. At ambient condition, $CeVO_4$ zircon structure contains two formula units per individual primitive cell. Group theory analysis predicted 12 Raman-active modes of $2A_{1g} + 4B_{1g} + B_{2g} + 5E_g$ which are classified into internal (ν_1–ν_4) and external (translational (T) and rotational (R)) modes of VO_4 units [10, 26]. Figure 3 a shows Raman spectrum of the as-prepared $CeVO_4$ sample with 450 °C calcination over wavenumber range of 100–1000 cm^{-1}. The highest intensity Raman peak at 857 cm^{-1} was specified as the internal symmetric-stretching $\nu_1(A_{1g})$ mode [10, 14, 26]. The sharp and shoulder peaks at 783 and 793 cm^{-1} are attributed to the asymmetric-stretching $\nu_3(E_g)$ and $\nu_3(B_{1g})$ modes, respectively. Those Raman peaks at 467 and 383 cm^{-1} are associated with the $\nu_4(B_{2g})$ and $\nu_2(B_{1g})$ deformation [10, 14, 26]. The external modes of $CeVO_4$ vibration are below 250 cm^{-1} [10].

The FTIR spectrum of as-prepared $CeVO_4$ sample with 450 °C calcination (Fig. 3b) shows IR bands at 772 cm^{-1} and 441 cm^{-1} which are attributed to the V–O stretching mode of VO_4 tetrahedral units and Ce–O stretching vibration of $CeVO_4$ lattice. The results indicate the formation of *tetragonal* zircon-type $CeVO_4$ structure [2, 17, 18, 26]. The observed broad band at 3200–3400 cm^{-1} is assigned as the OH stretching vibration of physically adsorbed water on the surface of as-prepared $CeVO_4$ sample [2, 3, 17, 18, 26].

Effect of calcination temperature at 450–600 °C on morphology and size of as-synthesized $CeVO_4$ samples was characterized by SEM as the results shown in Fig. 4. In this research, all samples were composed of particles with different size controlled by calcination temperature. SEM images show particles with the size of nanoscale range of 30–50 nm for $CeVO_4$ with 450 °C calcination and 80–120 nm for $CeVO_4$ with 500 °C calcination. At the calcination temperature higher than 500 °C, $CeVO_4$ nanoparticles grew up and became microparticles with the size ranges of 500–800 nm and 800–1500 nm for $CeVO_4$ with 550 and 600 °C calcination, respectively. Upon increasing in calcination temperature, the particles were enlarged and the size distribution became more non-uniform.

Figure 5 shows TEM images and SAED patterns of as-synthesized $CeVO_4$ samples with 450 and 500 °C calcination. The samples were composed of nanoparticles with particle size of 20–40 nm and 80–120 nm for the as-synthesized $CeVO_4$ samples with 450 and 500 °C calcination. The SEAD patterns of as-synthesized samples with 450 and 500 °C calcination show diffraction ring patterns of the (101), (200), (211), (112), (220), and (202) planes of $CeVO_4$ polycrystal.

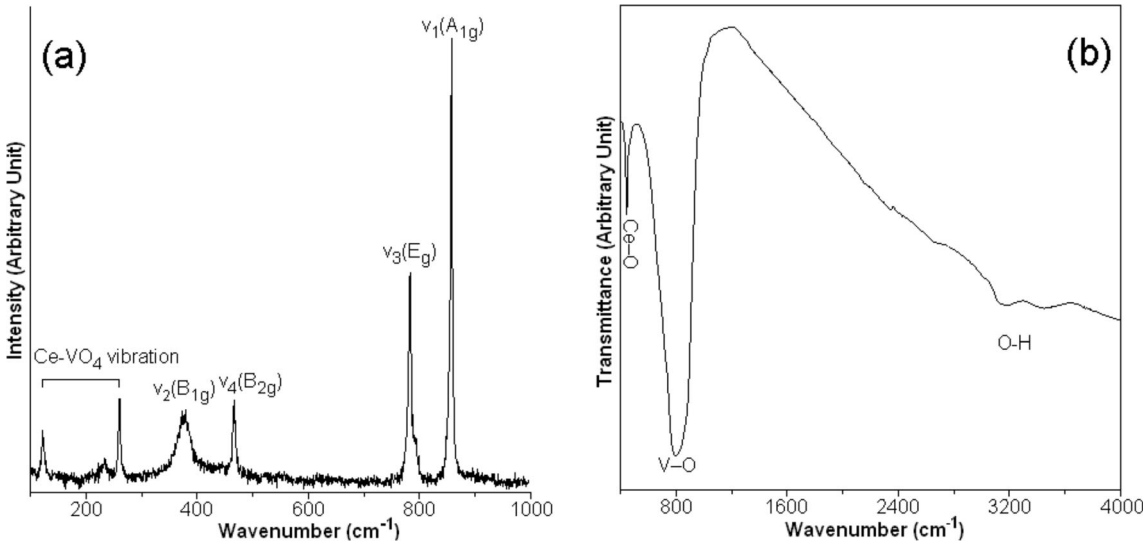

Fig. 3 **a** Raman and **b** FTIR spectra of $CeVO_4$ sample synthesized by sol-gel method and followed by 450 °C calcination for 2 h in ambient air

The photocatalytic performance of as-synthesized $CeVO_4$ with 450–600 °C calcination was investigated through photodegradation of MB solution under UV light irradiation. Figure 6 shows absorption spectra of MB solution over $CeVO_4$ with 450 °C and 600 °C calcination within regular time interval under UV light irradiation. The maximum intensity of absorption MB peak at 664 nm over as-synthesized $CeVO_4$ with 450 °C and 600 °C calcination gradually decreases with the increase of UV irradiation time. At the end of 120-min test, the absorption peak of MB almost disappeared for $CeVO_4$ with 450 °C calcination. This indicates that MB was rapidly photodegraded by $CeVO_4$ with 450 °C calcination under UV light irradiation. The maximum intensity of MB absorption peak at 664 nm was blue shifted to 658 nm caused by demethylation of MB under photocatalytic reaction [27–29].

Figure 7a shows photodegradation of MB over $CeVO_4$ with 450–600 °C calcination under UV light irradiation. Clearly, photodegradation of MB over as-prepared $CeVO_4$ sample with 450 °C calcination is 94.58% within 120 min under UV light irradiation. This indicates that the $CeVO_4$ photocatalyst exhibits an obvious simulated UV light-driven

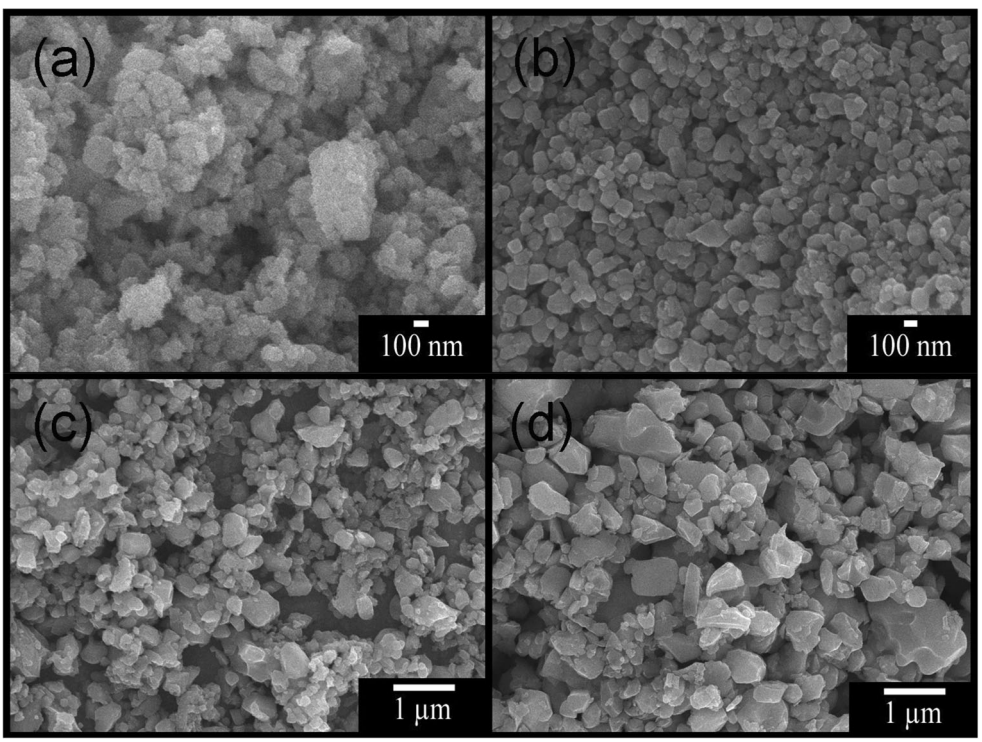

Fig. 4 SEM images of $CeVO_4$ samples synthesized by sol-gel method and followed by high temperature calcination at (**a**) 450 °C, (**b**) 500 °C, (**c**) 550 °C, and (**d**) 600 °C in ambient air

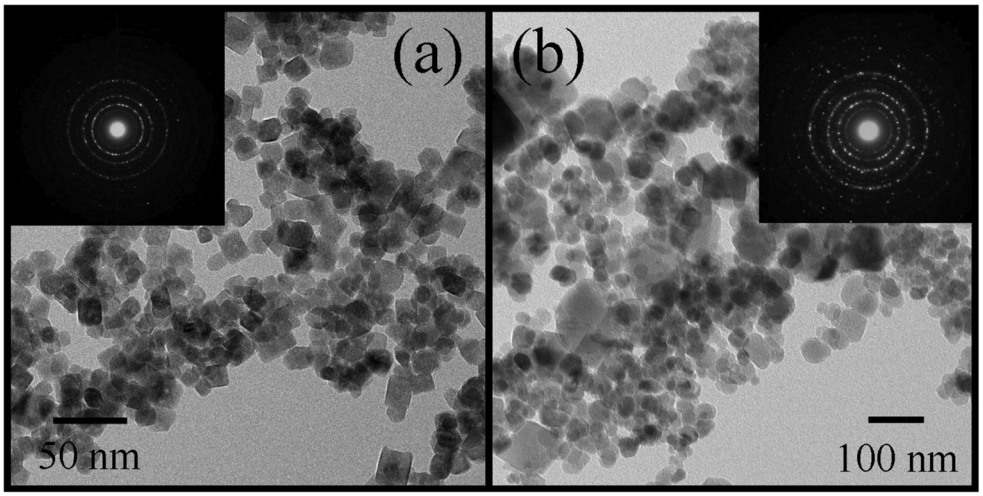

Fig. 5 TEM images and SAED patterns of $CeVO_4$ samples synthesized by sol-gel method and followed by high temperature calcination at (**a**) 450 °C and (**b**) 500 °C in ambient air

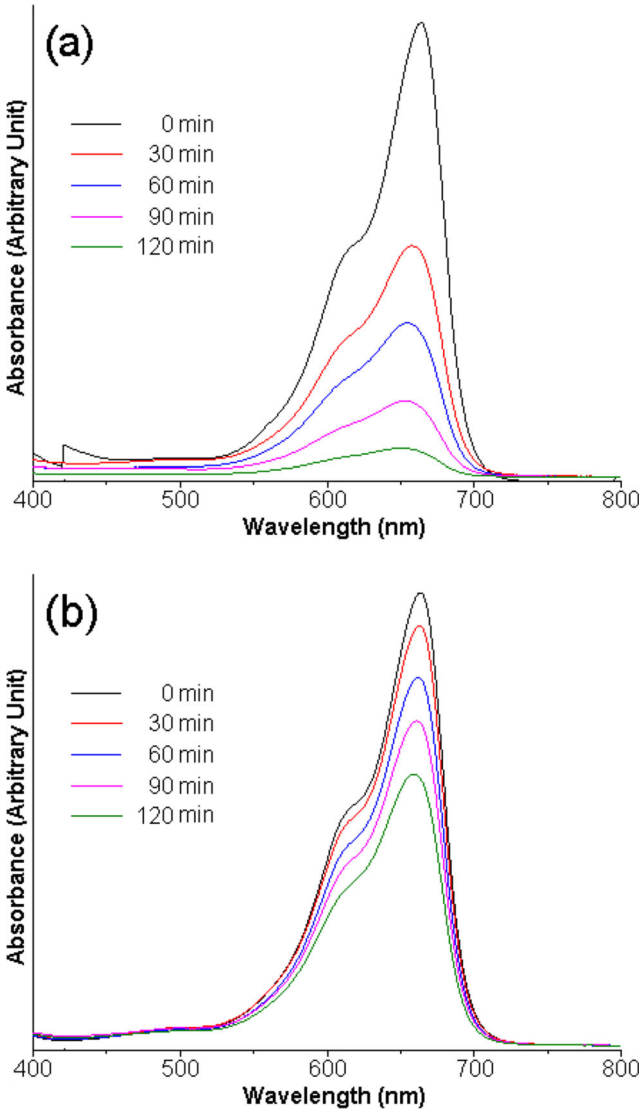

Fig. 6 UV–visible absorption of MB solutions containing $CeVO_4$ samples synthesized by sol-gel method and followed by high temperature calcination at (**a**) 450 °C and (**b**) 600 °C in ambient air

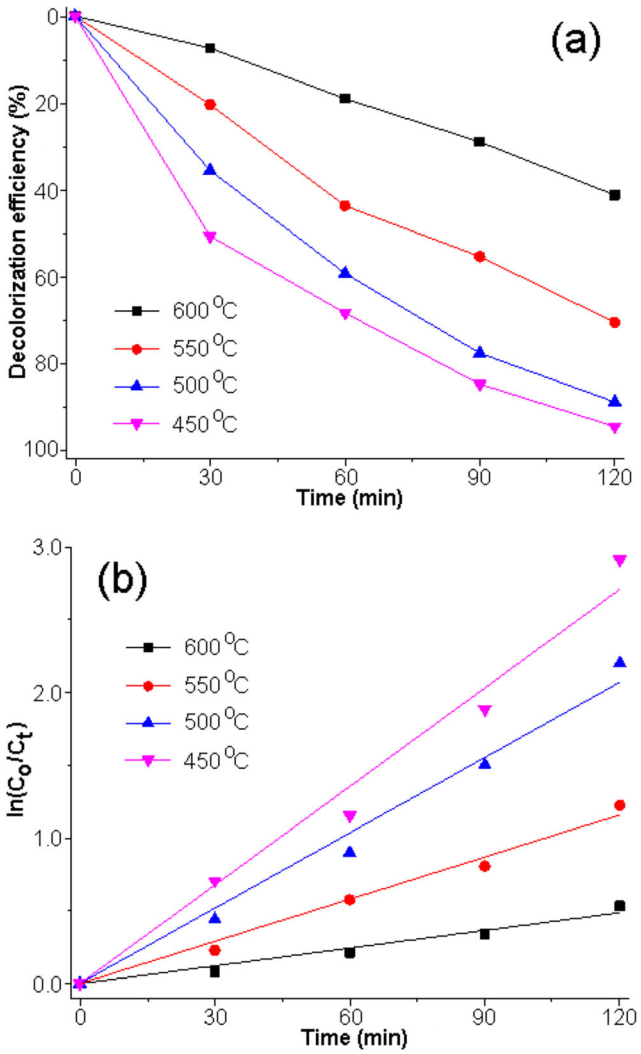

Fig. 7 **a** Decolorization efficiency and **b** reaction kinetics for photodegradation of MB over $CeVO_4$ samples synthesized by sol-gel method and followed by 450–600 °C calcination in ambient air

photocatalytic activity toward the MB dye degradation. The photodegradation of MB over $CeVO_4$ with 600 °C calcination was decreased to 41.29%. The phenomenon is attributed to relate with the particle size of $CeVO_4$ prepared using sol-gel method and followed by high temperature calcination. Among them, $CeVO_4$ with 450 °C calcination has the highest photocatalytic activity. Probably, this sample has the highest available surface active sites for photodegradation of MB under UV light irradiation [1, 15, 27, 28]. Figure 7 b shows linear fitting curves of $\ln(C_o/C_t)$ versus irradiation time (t) of $CeVO_4$ with 450–600 °C calcination under UV light irradiation. The curves follow the Langmuir–Hinshelwood kinetics as follows.

$$\ln(C_o/C_t) = kt \quad (2)$$

C_o and C_t are the MB concentrations at irradiation time of 0 and t, and k is the pseudo-first-order rate constant of MB photodegradation [3, 4, 28]. They show the linear lines with $R^2 > 0.9$ which certifies that the photocatalytic reaction follows pseudo-first-order kinetics [3, 4, 28]. The calculated k values are about 0.0226, 0.0172, 9.77×10^{-3}, and 1.51×10^{-3} min^{-1} for $CeVO_4$ with 450, 500, 550, and 600 °C calcination, respectively.

Ethylenediaminetetraacetic acid disodium salt (EDTA-2Na), p-benzoquinone (BQ), and isopropyl alcohol (IPA) for trapping hole (h^+), superoxide radical ($^{\bullet}O_2^-$), and hydroxyl radical ($^{\bullet}OH$) were used to explain the photodegradation of MB over $CeVO_4$ photocatalyst under UV light irradiation as the results shown in Fig. 8 [2, 29–33]. The degradation efficiency for MB was almost unchanged even after EDTA-2Na adding. Thus, the role of h^+ during photodegradation of MB over $CeVO_4$ photocatalyst is insignificant. When BQ and IPA were added to the photocatalytic system, the photodegradation of MB over the $CeVO_4$ photocatalyst was decreased to 45.25% and 21.35%, respectively. Thus, $^{\bullet}O_2^-$ and $^{\bullet}OH$ are the main active species for photodegradation of MB over the $CeVO_4$ photocatalyst under UV light irradiation.

In order to understand MB dye degradation over the as-prepared $CeVO_4$ photocatalyst, a photocatalytic mechanism was proposed according to the following. When $CeVO_4$ photocatalyst was irradiated by photon with energy > E_g, photo-excited electrons and photo-induced holes were in conduction and valence bands, respectively. Subsequently, active radicals were produced and degraded MB by transforming MB into CO_2 and H_2O described by the following [1, 15, 34, 35].

$$CeVO_4 + h\nu \rightarrow e^- + h^+ \quad (3)$$

$$e^- + O_2 \rightarrow {}^{\bullet}O_2^- \quad (4)$$

$$^{\bullet}O_2^- + H_2O \rightarrow HO_2 + OH^- \quad (5)$$

$$2HO_2 \rightarrow O_2 + H_2O_2 \quad (6)$$

$$H_2O_2 + {}^{\bullet}O_2^- \rightarrow {}^{\bullet}OH + OH^- + O_2 \quad (7)$$

$$h^+ + OH^- \rightarrow {}^{\bullet}OH \quad (8)$$

$$^{\bullet}O_2^- + \text{dye} \rightarrow \text{degradation products} \quad (9)$$

$$^{\bullet}OH + \text{dye} \rightarrow \text{degradation products} \quad (10)$$

The recycle photocatalytic experiment for photodegradation of MB dye over $CeVO_4$ under UV light irradiation was performed as the results shown in Fig. 9. At the end of five-recycle run, photodegradation of MB over the reused $CeVO_4$ photocatalyst was 91.25%. Thus, the stability of $CeVO_4$ photocatalyst is extremely good for photodegradation of MB dye under UV light irradiation.

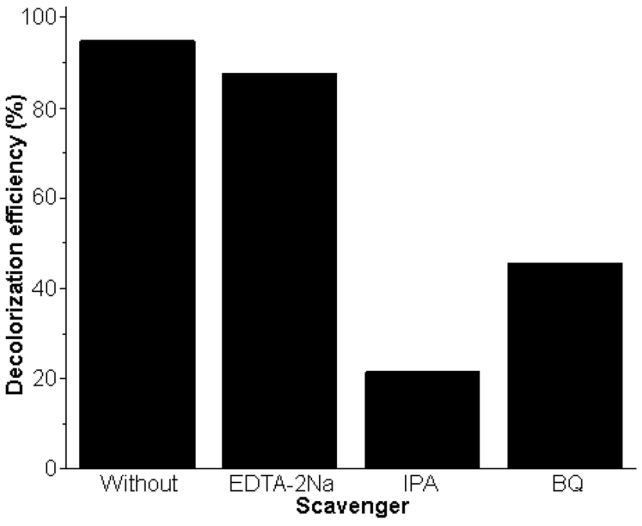

Fig. 8 Decolorization efficiency for photodegradation of MB solutions containing different scavengers over $CeVO_4$ photocatalyst with 450 °C calcination comparing with that for photodegradation of MB solution without a scavenger

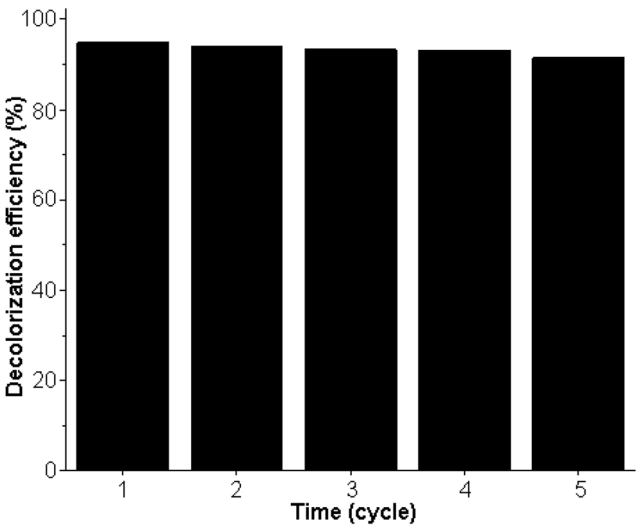

Fig. 9 Decolorization efficiency for photodegradation of MB over reused $CeVO_4$ nanoparticles synthesized by sol-gel method and followed by 450 °C calcination in ambient air

Conclusions

In summary, $CeVO_4$ as UV light-driven photocatalyst was synthesized by sol-gel method using tartaric acid as a complexing reagent and followed by 450–600 °C calcination for 2 h in ambient air. The photocatalytic properties of as-synthesized $CeVO_4$ samples were investigated by monitoring through MB degradation under UV light irradiation. In this study, $CeVO_4$ with 450 °C calcination shows the highest photocatalytic activity for MB degradation of 94.58% within 120 min under UV light irradiation. The main active species used for degradation of MB were $^{\bullet}O_2^-$ and $^{\bullet}OH$. The test for photocatalytic stability showed that $CeVO_4$ with 450 °C calcination is a promising candidate for wastewater treatment.

Funding We wish to thank the Center of Excellence in Materials Science and Technology, Chiang Mai University, for the financial support under the administration of Materials Science Research Center, Faculty of Science, Chiang Mai University, Thailand.

References

1. Ameri, V., Eghbali-Arani, M., Pourmasoud, S.: New route for preparation of cerium vanadate nanoparticles with different morphology and investigation of optical and photocatalytic properties, J. Mate.r Sci.: Mater. Electron. **28** (2017) 18835–18841
2. Yang, X., Zuo, W., Li, F., Li, T.: Surfactant-free and controlled synthesis of hexagonal $CeVO_4$ nanoplates: Photocatalytic activity and superhydrophobic property. ChemistryOpen. **4**, 288–294 (2015)
3. Phuruangrat, A., Thongtem, S., Thongtem, T.: Ultrasonic-assisted synthesis and photocatalytic performance of ZnO nanoplates and microflowers. Mater Des. **107**, 250–256 (2016)
4. Phuruangrat, A., Dumrongrojthanath, P., Yayapao, O., Thongtem, T., Thongtem, S.: Solvothermal synthesis and photocatalytic properties of CdS nanowires under UV and visible irradiation. Mater. Sci. Semicond. Process. **26**, 329–335 (2014)
5. Sharma, J.N., Pattadar, D.K., Mainali, B.P., Zamborini, F.P.: Size determination of metal aanoparticles based on electrochemically measured surface-area-to-volume ratios. Anal. Chem. **90**, 9308–9314 (2018)
6. Jin, R., Liu, C., Sun, L., Zhang, Z., Chen, G.: Solvothermal synthesis of yolk–shell $CeVO_4$/C microspheres as a high-performance anode for lithium-ion Bbtteries. Chem. Electro. Chem. **3**, 644–649 (2016)
7. Moussa, M., Djermouni, M., Kacimi, S., Azzouz, M., Dahani, A., Zaoui, A.: First-principles calculations of structural, magnetic phase stability and electronic properties of RVO_4 compounds. Comput. Mater. Sci. **68**, 361–366 (2013)
8. Bishnoi, S., Chawla, S.: Enhancement of $GdVO_4$:Eu^{3+} red fluorescence through plasmonic effect ofsilver nanoprisms on Si solar cell surface. J Appl Res Tech. **15**, 102–109 (2017)
9. He, J., Zhao, J., Run, Z., Sun, M., Pang, H.: Ultrathin cerium orthovanadate nanobelts for high-performance flexible all-solid-dtate asymmetric supercapacitors. Chem. Asian. J. **10**, 338–343 (2015)
10. Denisova, L.T., Chumilina, L.G., Kargin, Y.F., Denisov, V.M.: Synthesis of the $CeVO_4$ orthovanadate and its heat capacity in the range 350–1000 K. Inorg. Mater. **52**, 44–47 (2016)
11. Wang, Y., Zuo, R., Zhang, C., Zhang, J., Zhang, T.: Low-temperature-fired $ReVO_4$ (re = La, Ce) microwave dielectric ceramics. J. Am. Ceram. Soc. **98**, 1–4 (2015)
12. Ding, J., Liu, X., Wang, M., Liu, Q., Sun, T., Jiang, G., Tang, Y.: Controlled synthesis of $CeVO_4$ hierarchical hollow microspheres with tunable hollowness and their efficient photocatalytic activity. CrystEngComm. **20**, 4499–4505 (2018)
13. Guang, L., Xuejun, Z., Fei, W., Hui, W., Wei, L.: Facile fabrication of $CeVO_4$ microspheres with efficient visible light photocatalytic activity. Mater. Lett. **195**, 168–171 (2017)
14. Zain, J.H., Grover, V., Ramkumar, J., Bhattacharyya, K., Tyagi, A.K.: Mo-substituted $CeVO_4$ system: solid solution formation and implications on sorption behavior. J. Mater. Sci. **50**, 5690–5704 (2020)
15. Rahimi-Nasrabadi, M., Ahmadi, F., Fosooni, A.: Influence of capping agents additives on morphology of $CeVO_4$ nanoparticles and study of their photocatalytic properties. J. Mater. Sci. Mater. Electron. **28**, 537–542 (2017)
16. Mahapatra, S., Nayak, S.K., Madras, G., Row, T.N.G.: Microwave synthesis and photocatalytic activity of nano lanthanide (Ce, Pr, and Nd) orthovanadates. Ind. Eng. Chem. Res. **47**, 6509–6516 (2008)
17. Ekthammathat, N., Thongtem, T., Phuruangrat, A., Thongtem, S.: Synthesis and characterization of $CeVO_4$ by microwave radiation method and its photocatalytic activity, J. Nanomater. 2013 (2013) 1–7 Article ID 434197
18. Ghotekar, S., Pansambal, S., Pagar, K., Pardeshi, O., Oza, R.: Synthesis of $CeVO_4$ nanoparticles using sol-gel auto combustion method and their antifungal activity. Nanochem. Res. **3**, 189–196 (2018)
19. Muthee, D.K., Dejene, B.F.: The effect of tetra isopropyl orthotitanate (TIP) concentration on structural, and luminescence properties of titanium dioxide nanoparticles prepared by sol-gel method. Mater. Sci. Semicond. Process. **106**, 104783 (2020)
20. Triyono, D., Hanifah, U., Laysandra, H.: Structural and optical properties of mg-substituted $LaFeO_3$ nanoparticles prepared by a sol-gel method. Results Phys. **16**, 102995 (2020)
21. Huang, L., Sun, Y., Li, M., Yi, Y., Jiang, L., Fang, L.: Sol-gel derived Al and Ga co-doped ZnO nanoparticles: structural, morphological and optical investigation. Optik. **192**, 162942 (2019)
22. Jeevanandam, J., Chan, Y.S., Danquah, M.K.: Effect of gelling agent and calcination temperature in sol–gel synthesized MgO nanoparticles. Prot. Met. Phys. Chem. Surf. **55**, 288–301 (2019)
23. Mastuli, M.S., Kamarulzaman, N., Nawawi, M.A., Mahat, A.M., Rusdi, R., Kamarudin, N.: Growth mechanisms of MgO nanocrystals via a sol-gel synthesis using different complexing agents. Nanoscale. Res. Lett. **9**, 134 (2014)
24. A. Modwi, M.A. Abbo, E.A. Hassan, A. Houas, Effect of annealing on physicochemical and photocatalytic activity of Cu5% loading on ZnO synthesized by sol–gel method, J. Mater. Sci.: Mater. Electron. 27 (2016) 12974–12984
25. Powder Diffract. File, JCPDS-ICDD, 12 Campus Boulevard, Newtown Square, PA 19073–3273, **U.S.A.**, (2001)
26. Othman, I., Zain, J.H., Haija, M.A., Banat, F.: Catalytic activation of peroxymonosulfate using $CeVO_4$ for phenol degradation: an insight into the reaction pathway. Appl. Catal. B. **266**, 118601 (2020)
27. Sa-nguanprang, S., Phuruangrat, A., Thongtem, T., Thongtem, S.: Synthesis, analysis, and photocatalysis of Mg-doped ZnO nanoparticles. Russ. J. Inorg. Chem. **64**, 1841–1848 (2019)
28. Sa-nguanprang, S., Phuruangrat, A., Karthik, K., Thongtem, S., Thongtem, T.: Tartaric acid-assisted precipitation of visible light-driven Ce-doped ZnO nanoparticles used for photodegradation of methylene blue. J. Aust. Ceram. Soc. **56**, 1029–1041 (2020)
29. Rahmani, M., Sedaghat, T.: A facile sol–gel process for synthesis of $ZnWO_4$ nanopartices with enhanced band gap and study of ots

photocatalytic activity for degradation of methylene blue. J. Inorg. Organomet. Polym. Mater. **29**, 220–228 (2019)
30. Venkatesh, D., Pavalamalar, S., Anbalagan, K.: Selective photodegradation on dual dye system by recoverable nano SnO_2 photocatalyst. J. Inorg. Organomet. Polym. Mater. **29**, 939–953 (2019)
31. Tang, Q., Wu, W., Zhang, H., Luo, J., Zhang, B., Guo, X., Jia, J., Cao, J.: In situ ion exchange synthesis of cauliflower-like $AgBr/Ag_3PO_4$/sulfonated polystyrene sphere heterojunction photocatalyst with enhanced photocatalytic activity. J. Inorg. Organomet. Polym. Mater. **29**, 1154–1159 (2019)
32. Liu, C., Zhang, X., Wu, J., Meng, G., Guo, X., Liu, Z.: One-pot synthesis of visible-light-driven Ag/Ag_3PO_4 photocatalyst immobilized on exfoliated montmorillonite by clay-mediated in situ reduction. Appl. Phys. A. Mater. Sci. Process. **122**, 946 (2016)
33. Wang, Q., Yu, S., Qin, W., Wu, X.: Isopropanol-assisted synthesis of highly stable $MAPbBr_3$/p-g-C_3N_4 intergrowth composite photocatalysts and their interfacial charge carrier dynamics. Nanoscale. Adv. **23**, 274–285 (2020)
34. Wang, S., Li, D., Yang, C., Sun, G., Zhang, J., Xia, Y., Xie, C., Yang, G., Zhou, M., Liu, W.: A novel method for the synthesize of nanostructured $MgFe_2O_4$ photocatalysts. J. Sol-Gel. Sci. Technol. **84**, 169–179 (2017)
35. Mishra, S., Priyadarshinee, M., Debnath, A.K., Muthe, K.P., Mallick, B.C., Das, N., Parhi, P.: Rapid microwave assisted hydrothermal synthesis cerium vanadate nanoparticle and its photocatalytic and antibacterial studies. J. Phys. Chem. Solids. **137**, 109211 (2020)